Applied Physics Letters ARTICLE scitation.org/journal/apl

3D ultrasound directed self-assembly of high aspect ratio particles: On the relationship between the number of transducers and their spatial arrangement

Cite as: Appl. Phys. Lett. **117**, 111904 (2020); doi: 10.1063/5.0025367
Submitted: 14 August 2020 · Accepted: 7 September 2020 ·
Published Online: 18 September 2020

M. Prisbrey,[1] F. Guevara Vasquez,[2] and B. Raeymaekers[1,a)]

AFFILIATIONS

[1]Department of Mechanical Engineering, University of Utah, Salt Lake City, Utah 84112, USA
[2]Department of Mathematics, University of Utah, Salt Lake City, Utah 84112, USA

[a)]Author to whom correspondence should be addressed: bart.raeymaekers@utah.edu

ABSTRACT

Ultrasound directed self-assembly (DSA) enables noninvasively aligning high aspect ratio particles in three-dimensional (3D) user-specified orientations, which finds application in a myriad of engineering applications, including manufacturing engineered materials. However, the number of ultrasound transducers and their spatial arrangement limit the accuracy of the particle alignment with any 3D user-specified orientation. We define a set of 3D user-specified orientations and use numerical simulations to quantitatively evaluate the effect of the number of ultrasound transducers, their spatial arrangement including a sphere, cube, and two parallel plates, and the size of the spatial arrangement on the orientation error of a high aspect ratio particle in a standing ultrasound wave field. We demonstrate that a spatial arrangement of ultrasound transducers with more than two unique wave propagating directions is required to orient a high aspect ratio particle in 3D, and we determine that the orientation error decreases with the increasing number of unique wave propagation directions. Furthermore, we show that in a spherical arrangement of ultrasound transducers, the orientation error is independent of the size of the arrangement of transducers. This knowledge facilitates using ultrasound DSA as a fabrication method for engineered composite materials that derive their function from the location and orientation of particle inclusions.

External field-directed self-assembly (DSA) is the process by which discrete components organize into patterns due to interactions between themselves and their environment, driven by internal or external forces.[1] Thus, external field-DSA techniques enable non-invasively manipulating particles in a fluid medium, which finds applications in, for instance, cell-cell interaction studies,[2] microfluidic[3] and biomedical devices,[4] displays,[5] and fabrication of engineered materials with designer properties that derive from the location and orientation of patterns of particles embedded in the matrix material.[6–8]

External field DSA techniques employ an arrangement of transducers to establish a magnetic,[9] electric,[10] or ultrasound field[11–14] that manipulates particles into user-specified patterns. Tuning the operating parameters, number, and spatial arrangement of the transducers allows altering the external field and, thus, the locations where particles assemble. Magnetic and electric DSA typically require ultra-high field strength and ferromagnetic and electrically conductive particles, respectively,[15,16] which limits dimensional scalability and material choice. Alternatively, ultrasound DSA relies on the acoustic radiation force derived from the acoustic radiation potential associated with a standing ultrasound wave field to manipulate particles in a fluid medium. Ultrasound DSA drives particles, independent of their properties and geometry, to the locations of minimum acoustic radiation potential (ARP), which correspond to the nodes or antinodes of the wave field, depending on the relative compressibility of the particle and the fluid medium.[17] Additionally, low attenuation of ultrasound waves in low-viscosity fluids[18] such as water,[19] air,[20–22] and photopolymer resin[23] reduces the need for high field strengths, thus facilitating dimensional scalability.

Implementing ultrasound DSA in engineering applications requires knowing the relationship between the spatial arrangement of ultrasound transducers, their operating parameters (amplitude and phase), and the corresponding ultrasound wave field. Thus, we define the "forward" ultrasound DSA problem, which resolves the pattern of particles that assembles as a result of user-specified ultrasound

transducer operating parameters, and the "inverse" ultrasound DSA problem, which resolves the ultrasound transducer operating parameters required to assemble a user-specified pattern of particles. The forward ultrasound DSA problem is straightforward to solve analytically.[24] However, solving the inverse ultrasound DSA problem often requires complex numerical optimization techniques. Several solutions exist to the inverse ultrasound DSA problem to assemble user-specified patterns of spherical particles in 2D[25–27] and 3D,[28] and of high aspect ratio particles in 2D[29] and 3D[30] where the solution also accounts for the particle orientation.

The number and spatial arrangement of ultrasound transducers limit the ultrasound standing wave patterns and, thus, the patterns of particles that can be assembled. For spherical particles, a pattern is feasible if we can establish an ultrasound standing wave where the ARP minima coincide with the user-specified particle locations, whereas for high aspect ratio particles, the ARP minima must additionally align with the user-specified orientation.

It is not well understood how the number and spatial arrangement of ultrasound transducers relate to the portfolio of feasible user-specified patterns. The literature documents that common user-specified patterns of particles result from *a priori* knowledge of patterns of particles that are intuitive to assemble, such as a line pattern between parallel ultrasound transducers, or a rectangular pattern between orthogonally oriented ultrasound transducers.[25] Additionally, researchers use trial-and-error of the number and spatial arrangement of ultrasound transducers, until the desired user-specified pattern of particles is feasible to assemble, which is time consuming.[30] Alternatively, Guevara Vasquez *et al.* show theoretically that with a spherical arrangement of an infinite number of ultrasound transducers, any planar pattern of particles is feasible in the far-field, provided that the pattern of particles is a level-set of a 2D function with spatial frequency limited by the wavenumber.[31]

However, even for feasible user-specified patterns, deviations may exist between the user-specified and experimentally assembled or simulated patterns of particles; for instance, because of constructive or destructive interference in the ultrasound wave field, reflections, and manufacturing tolerances or misalignment of ultrasound transducers. A pattern error quantifies the deviation between the user-specified and any experimentally assembled or simulated pattern of particles. For spherical particles, it accounts for the deviation between the user-specified and actual particle locations,[25,28,32] whereas for high aspect ratio particles, the pattern error also accounts for the deviation between the user-specified and actual orientation.[29]

Few researchers have attempted to measure or simulate how the number and spatial arrangement of ultrasound transducers define the portfolio of feasible user-specified patterns. For instance, Grinenko *et al.* simulated that the area in which the location of a single spherical particle can be controlled increases with increasing number of ultrasound transducers arranged into a circle.[33] Greenhall *et al.* simulated ultrasound DSA of complex 2D patterns of spherical particles, such as a block "U" pattern, with 200 ultrasound transducers arranged into a square, and also qualitatively concluded that the number of ultrasound transducers affects the geometric complexity of the pattern of particles that one can assemble.[25] Prisbrey *et al.* also simulated ultrasound DSA of complex 3D patterns of spherical particles with 225 ultrasound transducers arranged into a sphere, confirming that Greenhall's observations in 2D also apply in 3D.[28] In another publication, Prisbrey *et al.* calculated that the orientation error associated with experimentally aligning a high aspect ratio particle in different 2D user-specified orientations decreases with the increasing number of ultrasound transducers (arranged into a circle).[29] Most recently, Prisbrey *et al.*[34] theoretically derived a solution to the inverse ultrasound DSA problem that computes the ultrasound transducer operating parameters required to align a single high aspect ratio particle in any 3D user-specified orientation, with any number and arrangement of ultrasound transducers. They experimentally validated their theory with a spherical arrangement of 24 ultrasound transducers and quantified the 3D orientation error between user-specified and experimentally obtained orientation.

The literature documents that increasing the number of ultrasound transducers increases the portfolio of feasible user-specified patterns in both 2D and 3D and decreases the pattern error between the user-specified and experimentally assembled or simulated pattern of particles, but no systematic evaluation exists. This knowledge is important to, e.g., use ultrasound DSA as a manufacturing method for engineered materials with designer properties. Hence, the objective of this work is to quantify how the number and spatial arrangement of ultrasound transducers affect the orientation error associated with 3D ultrasound DSA of a high aspect ratio particle. While this work does not yet provide a comprehensive solution, it contributes to understanding this important open problem in ultrasound DSA.

Figure 1 depicts the 3D user-specified orientation of the major axis of a high aspect ratio particle $\mathbf{e}_d$ (red), where

$$\mathbf{e}_d = \begin{bmatrix} \cos(\theta_d)\cos(\varphi_d) \\ \sin(\theta_d)\cos(\varphi_d) \\ -\sin(\varphi_d) \end{bmatrix}. \quad (1)$$

Here, θ_d is a rotation angle in the xy-plane and φ_d is a rotation angle in the xz-plane. We use the formulation of Prisbrey *et al.*[34] to solve the inverse ultrasound DSA problem and compute the operating parameters $\mathbf{v}^* = [v_{1,\ldots},v_{j,\ldots},v_{Nt}]^T$ of each ultrasound transducer j, required to align a single high aspect ratio particle in orientation $\mathbf{e}_d$ at the center $\mathbf{o}$ of any spatial arrangement of N_t ultrasound transducers. Here, $v_j = A_j e^{i\psi}{}_j$, where A_j and ψ_j are the amplitude and phase of the jth ultrasound transducer, respectively, and $i = (-1)^{1/2}$. The solution method uses constrained optimization to determine the optimal operating parameters $\mathbf{v}^*$ of the spatial arrangement of ultrasound transducers required to locally minimize the ARP U, minimize the curvature of U in the user-specified orientation κ_d, and maximize the curvature of U

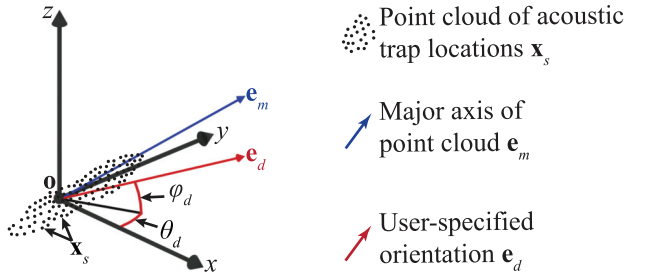

FIG. 1. 3D user-specified orientation $\mathbf{e}_d$ (red) of a high aspect ratio particle centered at $\mathbf{o}$ with point cloud of resulting acoustic trap locations $\mathbf{x}_s$ (black dots) and major axis of the point cloud $\mathbf{e}_m$.

in two orthogonal directions κ_i and κ_j simultaneously at multiple locations along $\mathbf{e}_d$.[34]

The ARP in a fluid medium with density ρ_0 and sound propagation speed c_0 is given as[17,35]

$$U = 2\Phi_1\left(|P|^2\right) - 2\Phi_2\left(\left|\frac{\partial P}{\partial x}\right|^2 + \left|\frac{\partial P}{\partial y}\right|^2 + \left|\frac{\partial P}{\partial z}\right|^2\right), \quad (2)$$

with the acoustic contrast factors

$$\Phi_1 = \frac{\pi r_p^3}{3}\left(\frac{1}{c_0^2\rho_0} - \frac{1}{c_p^2\rho_p}\right), \quad (3)$$

$$\Phi_2 = \pi r_p^3\left(\frac{\rho_p - \rho_0}{\omega_0\rho_0(\rho_0 + 2\rho_p)}\right), \quad (4)$$

where r_p is the length of the minor axis (thickness) of the high aspect ratio particle.

$P = \sum_{j=1}^{N_t} p_j$ is the total (complex) pressure at an arbitrary domain point $\mathbf{x}_l$, where we calculate the contribution of each jth ultrasound transducer (circular with radius a) as[36]

$$p_j = P_0\frac{J_1\left(k_0 a\sin(\theta_j)\right)}{k_0 a\sin(\theta_j)}\frac{e^{ik_0 r_j}}{r_j}v_j. \quad (5)$$

$k_0 = 2\pi/\lambda_0$ is the wavenumber, λ_0 is the wavelength of the ultrasound wave field, J_1 is the first order Bessel function of the first kind, P_0 is an ultrasound transducer property (pressure amplitude in Pa per volt peak-to-peak (Vpp) square excitation signal at a distance from the ultrasound transducer) that relates the pressure amplitude to the voltage amplitude driving the jth ultrasound transducer, r_j is the Euclidean distance between the jth ultrasound transducer and a domain point $\mathbf{x}_l$, and θ_j is the angle between the normal on the jth ultrasound transducer surface and $\mathbf{x}_l$.

Figure 1 also depicts a point cloud of acoustic trap locations $\mathbf{x}_s$ associated with the ultrasound wave field that results from applying $\mathbf{v}^*$ to all N_t ultrasound transducers. Specifically, $\mathbf{x}_s$ are the locations where the acoustic radiation force $\mathbf{F} = -\nabla U$ acting on a high aspect ratio particle with density ρ_p and sound propagation speed c_p equals zero and points toward $\mathbf{x}_s$ in the surrounding region, and where U is locally minimum. A cluster of acoustic trap locations in close proximity locate and orient a single high aspect ratio particle in the orientation established by the ultrasound wave field. Thus, the major axis $\mathbf{e}_m$ (blue) of an ellipse fitted to the point cloud of acoustic trap locations $\mathbf{x}_s$ defines the 3D orientation of a high aspect ratio particle in the ultrasound wave field. Perfect alignment of the major axis of the high aspect ratio particle with the user-specified orientation exists when $\mathbf{e}_m = \mathbf{e}_d$. Hence, we define the orientation error γ between $\mathbf{e}_d$ and $\mathbf{e}_m$ as

$$\gamma = \arccos(\mathrm{e}_d \cdot \mathrm{e}_m). \quad (6)$$

We only consider the orientation error because we always locate the high aspect ratio particle at $\mathbf{o}$.

Figure 2 shows ultrasound transducers arranged into (a) a sphere, (b) a cube, and (c) two parallel planes and illustrates how we increase N_t from sparse to dense. We select these arrangements to represent configurations in which the primary wave propagation direction emitted from each ultrasound transducer is unique (sphere), points along three orthogonal axes (cube), and establishes a standing wave in one direction (parallel planes).

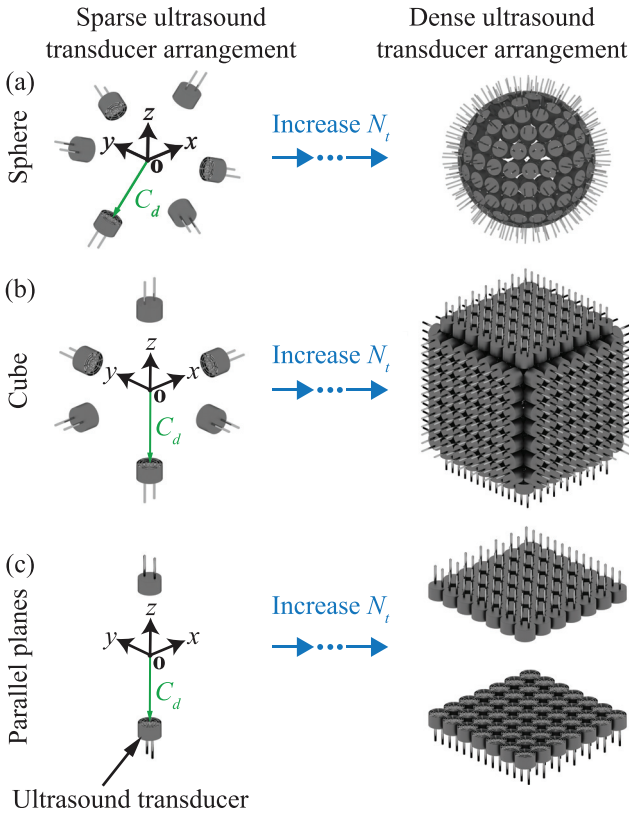

FIG. 2. Ultrasound transducers arranged into (a) a sphere, (b) a cube, and (c) two parallel planes, showing a sparse (left) and a dense configuration (right) and indicating the characteristic dimension C_d.

We maintain an equidistant ultrasound transducer spacing in the spherical arrangement,[37] whereas in the cube and parallel plane arrangements, we ensure that the normal on the ultrasound transducer surface at the center of each plane array intersects $\mathbf{o}$. For each spatial arrangement, we also vary the characteristic dimension C_d, which we define as the radius of the sphere, the distance from the center $\mathbf{o}$ to the planes of the cube, and distance from the center $\mathbf{o}$ to each plane, respectively. We simulate ultrasound transducers with radius $a = 4.5$ mm (type MURATA MA40S4S) with $\omega_0/2\pi = 40$ kHz, and orient a high aspect ratio expanded polystyrene (EPS) particle ($\rho_p = 25\,\mathrm{kg/m^3}$), with the average length of the major and minor axes being 4.2 mm and 2.1 mm in air.

We define 100 different user-specified orientations using combinations of θ_d and φ_d between 0° and 90° in 10° increments and determine the orientation error γ. We select $C_d/\lambda_0 = 3$, 6.5, 10, and 13.5 for each spatial arrangement to determine the effect of the size. The minimum $C_d/\lambda_0 = 3$ ensures that the center point $\mathbf{o}$ resides in the far-field region of the ultrasound wave field. Furthermore, we vary N_t for the sphere between $N_t = \{6, 99\}$, cube $N_t = \{6, 1014\}$, and parallel planes $N_t = \{2, 578\}$. Thus, we calculate 100 orientation errors for each spatial arrangement, for each characteristic dimension, and for each number of ultrasound transducers.

Figures 3(a)–3(c) show the average orientation error γ_a for the set of 100 user-specified orientations as a function of the number of

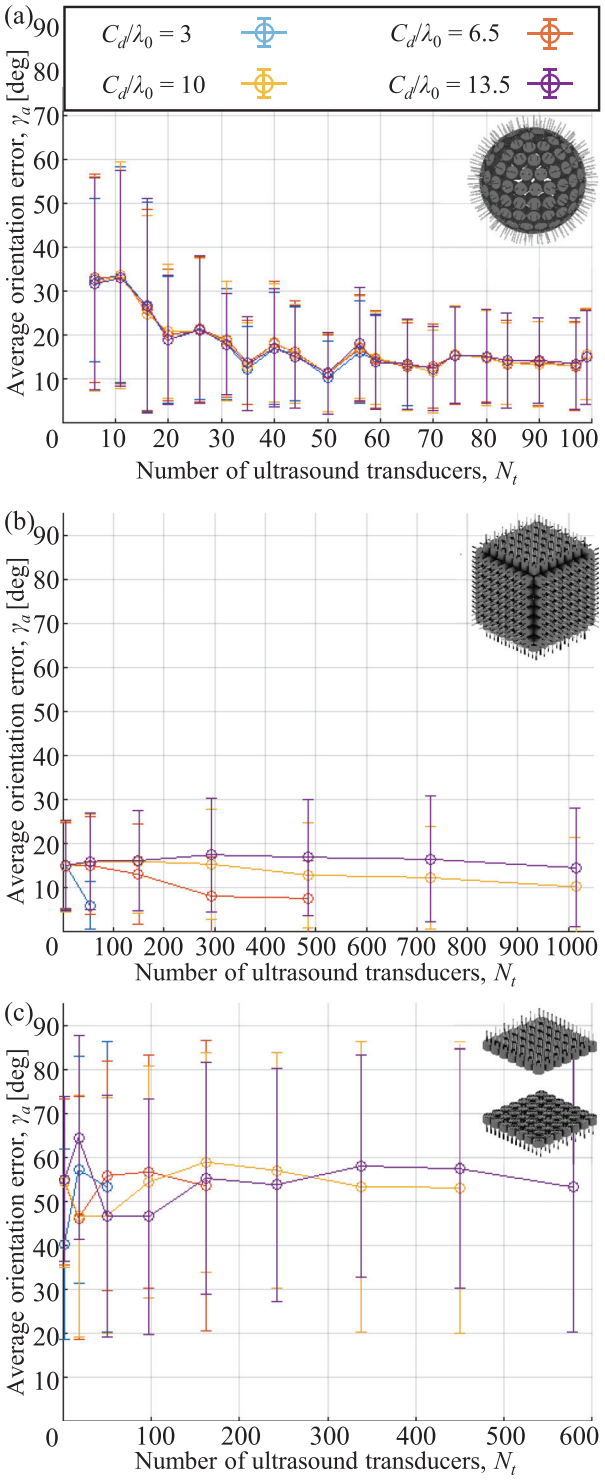

FIG. 3. Average orientation error γ_a for ultrasound transducers arranged into (a) a sphere, (b) a cube, and (c) parallel planes as a function of the number of ultrasound transducers N_t and characteristic dimension C_d/λ_0.

ultrasound transducers N_t and characteristic dimension C_d for ultrasound transducers arranged into (a) a sphere, (b) a cube, and (c) two parallel planes. The error bars represent one standard deviation of the orientation error. From Fig. 3(a), we observe that γ_a is almost independent of C_d/λ_0 but decreases with increasing N_t. The standard deviation of γ also decreases with increasing N_t, indicating that the accuracy increases. From Fig. 3(b), we observe that the γ_a increases with increasing C_d/λ_0 and decreases with increasing N_t. Furthermore, the standard deviation of γ is independent of N_t. From Fig. 3(c), we observe that the average and standard deviation of γ does not vary significantly with N_t or C_d/λ_0. We also note the high γ_a for the spatial arrangement of two parallel planes [Fig. 3(c)] compared to that of the sphere [Fig. 3(a)] and cube [Fig. 3(b)].

Figures 4(a)–4(c) show U resulting from implementing $\mathbf{v}*$ (from the solution to the inverse ultrasound DSA problem) in a square solution domain with length $2\lambda_0$ centered at $\mathbf{o}$, in the xz-plane, for $\theta_d = 0°$ and $\varphi_d = 30°$ (indicated by $\mathbf{e}_d$ in red), respectively, and for the spatial arrangement of sphere [Fig. 4(a)], cube [Fig. 4(b)], and two parallel planes [Fig. 4(c)]. We maintain N_t constant and vary C_d/λ_0 to illustrate how the minima of U (dark green), where a high aspect ratio particle aligns, evolve with increasing C_d/λ_0.

We observe from Fig. 4(a) that there is no difference between U for $C_d/\lambda_0 = 3$ and $C_d/\lambda_0 = 13.5$, which matches the observations of Fig. 3(a) that show that the γ_a is independent of C_d/λ_0. The minima (dark green) of U at $\mathbf{o}$ result from ultrasound waves emitted from ultrasound transducers that have a unique propagation direction.

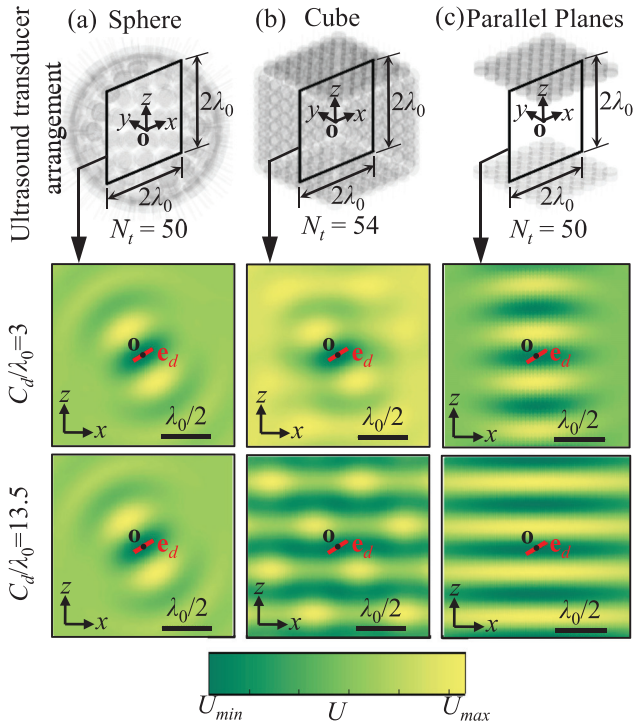

FIG. 4. ARP U in (a) sphere, (b) cube, and (c) parallel plane ultrasound transducer arrangements for $C_d/\lambda_0 = 3$ and 13.5 and for $\theta_d = 0°$ and $\varphi_d = 30°$.

Thus, the ability to align a high aspect ratio particle in a user-specified orientation in a spherical arrangement of ultrasound transducers is independent of the size of the sphere. In contrast, we qualitatively observe from Figs. 4(b) and 4(c) that the width of minima of U (dark green) increases in the x-direction, with increasing C_d/λ_0. Furthermore, we observe that the inclination of the minima of U approaches zero, despite imposing $\theta_d = 0^\circ$ and $\varphi_d = 30^\circ$ to the inverse ultrasound DSA solution. The Huygens principle causes the ultrasound waves emitted from each ultrasound transducer to approach a plane wave, with the increasing distance from the source. Hence, in spatial arrangements that comprise orthogonal or parallel-oriented plane arrays of ultrasound transducers, the ability to align a high aspect ratio particle in a user-specified orientation that is not parallel to the ultrasound transducers decreases with the increasing size. This explains the increasing γ_a with increasing C_d/λ_0 for the cube spatial arrangement [Fig. 3(b)]. The ability to orient a high aspect ratio particle with just two parallel arrays of ultrasound transducers is even more compromised as evidenced by the high γ_a, independent of C_d/λ_0 and N_t [Fig. 3(c)].

Figures 5(a)–5(c) show U resulting from implementing $\mathbf{v}^*$ (from the solution to the inverse ultrasound DSA problem) in a square solution domain with length $2\lambda_0$ centered at $\mathbf{o}$, in the xz-plane, for $\theta_d = 0^\circ$ and $\varphi_d = 30^\circ$ (indicated by $\mathbf{e}_d$ in red), respectively, and for the sphere [Fig. 5(a)], cube [Fig. 5(b)], and two parallel planes' [Fig. 5(c)] spatial arrangement of ultrasound transducers. We maintain a constant C_d/λ_0 and vary N_t to illustrate how the minima of U (dark green), where a high aspect ratio particle aligns, evolve with increasing N_t.

We qualitatively observe from Fig. 5(a) that increasing N_t for the spherical arrangement improves the alignment of the minima of U (dark green) at $\mathbf{o}$ with the user-specified direction $\mathbf{e}_d$. However, the improvement between $N_t = 6$ and $N_t = 50$ does not continue beyond $N_t = 50$. Thus, for a spherical arrangement with sufficient ultrasound transducers, γ_a is independent of N_t. In contrast, we qualitatively observe from Figs. 5(b) and 5(c) that increasing N_t in the cube and two parallel plane arrangements does not improve the alignment of the minima of U (dark green) at $\mathbf{o}$ with $\mathbf{e}_d$. However, it decreases the width of the minima of U (dark green) in the x-direction.

We have assumed that the ultrasound waves emitted from the ultrasound transducers do not reflect off nearby surfaces. However, reflections could affect a practical implementation and orientation error. While we assumed a massless particle, one must ensure that the curvature of U is sufficiently large in the direction of gravity to support the particle,[34] by maximizing the curvature of U in the direction of gravity, in addition to optimizing the remaining terms in the objective function.

We conclude that to minimize the orientation error of a high aspect ratio particle, it is important to use an arrangement of ultrasound transducers with wave sources oriented in different directions because the Huygens principle causes the ultrasound waves emitted from each ultrasound transducer to approach a plane wave, with the increasing distance from the source. Hence, in spatial arrangements that comprise orthogonal or parallel-oriented plane arrays of ultrasound transducers, the ability to align a high aspect ratio particle in a user-specified orientation that is not parallel to the ultrasound transducers decreases with the increasing size. In contrast, in a spherical arrangement, each ultrasound transducer is oriented in a unique direction. For that reason, the orientation error is independent of the size and decreases with increasing ultrasound transducers.

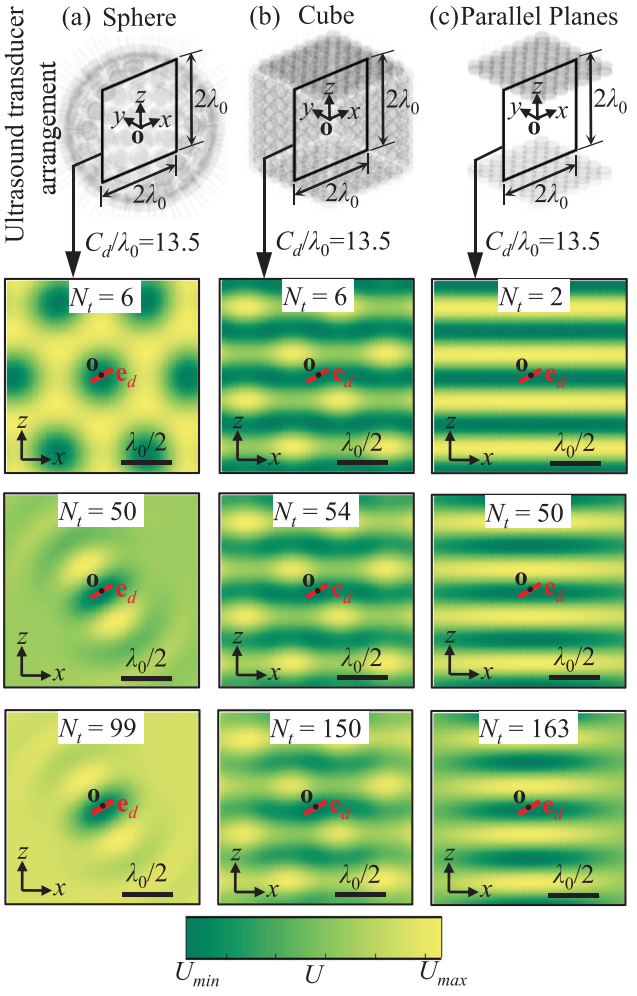

FIG. 5. ARP U in (a) sphere, (b) cube, and (c) parallel plane ultrasound transducer arrangements for $C_d/\lambda_0 = 13.5$, user-specified angles $\theta_d = 0^\circ$ and $\varphi_d = 30^\circ$ and for increasing N_t.

This research was supported by the Army Research Office under Contract No. W911NF-16-1-0457.

DATA AVAILABILITY

The data that support the findings of this study are available from the corresponding author upon reasonable request.

REFERENCES

[1]M. Grzelczak, J. Vermant, E. M. Furst, and L. M. Liz-Marzán, ACS Nano **4**, 3591 (2010).
[2]Y. Yamakoshi, Y. Koitabashi, N. Nakajima, and T. Miwa, Jpn. J. Appl. Phys., Part 1. **45**, 4712 (2006).
[3]B. Jung, K. Fisher, K. D. Ness, K. A. Rose, and R. P. Mariella, Anal. Chem. **80**, 8447 (2008).
[4]M. Evander and J. Nilsson, Lab Chip **12**, 4667 (2012).
[5]R. Hirayama, D. Martinez Plasencia, N. Masuda, and S. Subramanian, Nature **575**, 320 (2019).
[6]J. N. Coleman, U. Khan, W. J. Blau, and Y. K. Gun'ko, Carbon **44**, 1624 (2006).

[7]V. M. Shalaev, Nat. Photonics **1**, 41 (2007).
[8]S. J. Corbitt, M. Francoeur, and B. Raeymaekers, J. Quant. Spectrosc. Radiat. Transfer **158**, 3 (2015).
[9]S. K. Smoukov, S. Gangwal, M. Marquez, and O. D. Velev, Soft Matter **5**, 1285 (2009).
[10]Q. Wang, J. Dai, W. Li, Z. Wei, and J. Jiang, Comp. Sci. Technol. **68**, 1644 (2008).
[11]K. Niendorf and B. Raeymaekers, Composites, Part A **129**, 105713 (2020).
[12]D. Baresch, J.-L. Thomas, and R. Marchiano, Phys. Rev. Lett. **116**, 024301 (2016).
[13]D. Baresch, J.-L. Thomas, and R. Marchiano, Phys. Rev. Lett. **121**, 074301 (2018).
[14]J. Greenhall, F. Guevara Vasquez, and B. Raeymaekers, Appl. Phys. Lett. **105**, 144105 (2014).
[15]M. Fujiwara, E. Oki, M. Hamada, Y. Tanimoto, I. Mukouda, and Y. Shimomura, J. Phys. Chem. A **105**, 4383 (2001).
[16]P. V. Kamat, K. G. Thomas, S. Barazzouk, G. Girishkumar, K. Vinodgopal, and D. Meisel, J. Am. Chem. Soc. **126**, 10757 (2004).
[17]L. P. Gor'kov, Sov. Phys.-Dokl. **6**, 773 (1962).
[18]L. E. Kinsler, A. R. Frey, A. B. Coppens, and J. V. Sanders, *Fundamentals of Acoustics* (John Wiley, New York, 2000).
[19]C. R. P. Courtney, B. W. Drinkwater, C. E. M. Demore, S. Cochran, A. Grinenko, and P. D. Wilcox, Appl. Phys. Lett. **102**, 123508 (2013).
[20]Y. Ochiai, T. Hoshi, and J. Rekimoto, PLoS One **9**, e97590 (2014).
[21]A. Marzo, A. Barnes, and B. W. Drinkwater, Rev. Sci. Instrum. **88**, 085105 (2017).
[22]D. Foresti, M. Nabavi, M. Klingauf, A. Ferrari, and D. Poulikakos, Proc. Natl. Acad. U. S. A. **110**, 12549 (2013).
[23]J. Greenhall and B. Raeymaekers, Adv. Mater. Technol. **2**, 1700122 (2017).
[24]J. Greenhall, F. Guevara Vasquez, and B. Raeymaekers, Appl. Phys. Lett. **103**, 074103 (2013).
[25]J. Greenhall, F. Guevara Vasquez, and B. Raeymaekers, Appl. Phys. Lett. **108**, 103103 (2016).
[26]C. R. P. Courtney, C.-K. Ong, B. W. Drinkwater, A. L. Bernassau, P. D. Wilcox, and D. R. S. Cumming, Proc. R. Soc. A **468**, 337–360 (2011).
[27]A. L. Bernassau, C. R. P. Courtney, J. Beeley, B. W. Drinkwater, and D. R. S. Cumming, Appl. Phys. Lett. **102**, 164101 (2013).
[28]M. Prisbrey and B. Raeymaekers, Phys. Rev. Appl. **10**, 034066 (2018).
[29]M. Prisbrey and B. Raeymaekers, Phys. Rev. Appl. **12**, 014014 (2019).
[30]A. Marzo, S. A. Seah, B. W. Drinkwater, D. R. Sahoo, B. Long, and S. Subramanian, Nat. Commun. **6**, ncomms 8661 (2015).
[31]F. G. Vasquez and C. Mauck, SIAM J. Appl. Math. **78**, 1283 (2018).
[32]M. Prisbrey, J. Greenhall, F. Guevara Vasquez, and B. Raeymaekers, J. Appl. Phys. **121**, 014302 (2017).
[33]A. Grinenko, P. D. Wilcox, C. R. P. Courtney, and B. W. Drinkwater, Proc. R. Soc. A **468**, 3571 (2012).
[34]M. Prisbrey, F. G. Vasquez, and B. Raeymaekers, Phys. Rev. Appl. **14**, 024026 (2020).
[35]H. Bruus, Lab Chip **12**, 1014 (2012).
[36]J. D. N. Cheeke, *Fundamentals and Applications of Ultrasonic Waves* (CRC Press, Boca Raton, 2002).
[37]M. Deserno, *How to Generate Equidistributed Points on the Surface of a Sphere* (Max-Planck-Institut fur Polymerforschung, Mainz, 2004).